12-2014

Dependence of ablative ability of high-intensity focused ultrasound cavitation-based histotripsy on mechanical properties of agar

Jin Xu
Iowa State University

Timothy A. Bigelow
Iowa State University, bigelow@iastate.edu

Gabriel Davis
Iowa State University

Alex Avendano
Iowa State University

Pranav Shrotriya
Iowa State University, shrotriy@iastate.edu
See next page for additional authors

Dependence of ablative ability of high-intensity focused ultrasound cavitation-based histotripsy on mechanical properties of agar

Abstract
Cavitation-based histotripsy uses high-intensity focused ultrasound at low duty factor to create bubble clouds inside tissue to liquefy a region, and provides better fidelity to planned lesion coordinates and the ability to perform real-time monitoring. The goal of this study was to identify the most important mechanical properties for predicting lesion dimensions, among these three: Young's modulus, bending strength, and fracture toughness. Lesions were generated inside tissue-mimicking agar, and correlations were examined between the mechanical properties and the lesion dimensions, quantified by lesion volume and by the width and length of the equivalent bubble cluster. Histotripsy was applied to agar samples with varied properties. A cuboid of 4.5mm width (lateral to focal plane) and 6mm depth (along beam axis) was scanned in a raster pattern with respective step sizes of 0.75 and 3mm. The exposure at each treatment location was either 15, 30, or 60s. Results showed that only Young's modulus influenced histotripsy's ablative ability and was significantly correlated with lesion volume and bubble cluster dimensions. The other two properties had negligible effects on lesion formation. Also, exposure time differentially affected the width and depth of the bubble cluster volume.

Keywords
Mechanical Engineering, algae, bending strength, cavitation, elastic moduli, fracture, polysaccharides, tissue, ultrasonics, bubble clusters, high intensity focused ultrasound, lesion formation, real time monitoring, Young's Modulus, biomechanics

Disciplines
Electrical and Computer Engineering | Mechanical Engineering

Comments
The following article appeared in *Journal of the Acoustical Society of America* 136 (2014): 3018 and may be found at doi: 10.1121/1.4898426.

Authors
Jin Xu, Timothy A. Bigelow, Gabriel Davis, Alex Avendano, Pranav Shrotriya, Kevin Bergler, and Zhong Hu

Dependence of ablative ability of high-intensity focused ultrasound cavitation-based histotripsy on mechanical properties of agar

Jin Xu[a)]
Department of Mechanical Engineering, Iowa State University, Black Engineering Hall, Ames, Iowa 50011

Timothy A. Bigelow
Department of Electrical and Computer Engineering, Iowa State University, Coover Hall, Ames, Iowa 50011

Gabriel Davis, Alex Avendano, Pranav Shrotriya, and Kevin Bergler
Department of Mechanical Engineering, Iowa State University, Black Engineering Hall, Ames, Iowa 50011

Zhong Hu
Department of Electrical and Computer Engineering, Iowa State University, Coover Hall, Ames, Iowa 50011

(Received 3 August 2013; revised 15 August 2014; accepted 6 October 2014)

Cavitation-based histotripsy uses high-intensity focused ultrasound at low duty factor to create bubble clouds inside tissue to liquefy a region, and provides better fidelity to planned lesion coordinates and the ability to perform real-time monitoring. The goal of this study was to identify the most important mechanical properties for predicting lesion dimensions, among these three: Young's modulus, bending strength, and fracture toughness. Lesions were generated inside tissue-mimicking agar, and correlations were examined between the mechanical properties and the lesion dimensions, quantified by lesion volume and by the width and length of the equivalent bubble cluster. Histotripsy was applied to agar samples with varied properties. A cuboid of 4.5 mm width (lateral to focal plane) and 6 mm depth (along beam axis) was scanned in a raster pattern with respective step sizes of 0.75 and 3 mm. The exposure at each treatment location was either 15, 30, or 60 s. Results showed that only Young's modulus influenced histotripsy's ablative ability and was significantly correlated with lesion volume and bubble cluster dimensions. The other two properties had negligible effects on lesion formation. Also, exposure time differentially affected the width and depth of the bubble cluster volume. © *2014 Acoustical Society of America*.
[http://dx.doi.org/10.1121/1.4898426]

PACS number(s): 43.35.Ei, 43.25.Yw [OAS] Pages: 3018–3027

I. INTRODUCTION

Destruction of biological tissues by means of high-intensity focused ultrasound (HIFU) provides the prospect of safe noninvasive surgery, as extracorporeally delivered energy is constrained within a small focal volume, without harming the intervening tissue along the acoustic propagation path. The bioeffects harnessed to ablate the target tissue vary, with their individual dominance depending on the temporal focal intensity and pulsing scheme. For instance, using a continuous wave at an intensity of less than 1 kW/cm^2, localized thermal ablation of target tissues occurs, arising from accumulated heat in the focal zone and corresponding local temperature elevation of 13 °C or more (Clarke and Haar, 1997; Uchida *et al.*, 1998; Blana *et al.*, 2004; Damianou *et al.*, 2004; Orvieto *et al.*, 2009). At higher intensities, destructive effects derive from clouds of micron-sized cavitating bubbles inside the tissue (Xu *et al.*, 2007a; Xu *et al.*, 2007b; Wang *et al.*, 2010), or from transient boiling (in milliseconds) (Canney *et al.*, 2010; Maxwell *et al.*, 2012), depending upon the specific pulsing scheme. The HIFU technology using these two mechanisms to fractionate bulk tissues is termed *histotripsy*. Boiling histotripsy and cavitation histotripsy yield similar morphological characteristics of tissue damage, despite their different operational frequencies, pulse durations, and pulse repetition frequencies (PRFs).

Histotripsy (based on either mechanism) uses HIFU with high pulse-average intensity but low duty factor (~1%) to allow long cool-off times during intense ultrasound exposures. In this fashion, the minimized heat deposition reduces the necessity for a costly imaging method such as MRI to provide detailed temperature mapping to prevent undesired injury to surrounding tissues. Also, histotripsy is compatible with traditional ultrasound imaging and enables therapy to be monitored in real-time (Rabkin *et al.*, 2005; Parsons *et al.*, 2006), since temperature regulation is not as stringent in heating-based HIFU modality. Moreover, histotripsy is safe because of the narrow beam width in the focal plane (on the order of mm for the −3 dB zone which corresponds to larger than 50% peak intensity), and because of the sharply defined pressure threshold for bubble cloud generation in cavitation histotripsy (Bigelow *et al.*, 2009; Gateau *et al.*, 2011) or for tissue boiling within the acoustic burst in boiling histotripsy (Canney *et al.*, 2010). Therefore, the damage is highly likely to remain at the targeted region. In summary,

[a)]Author to whom correspondence should be addressed. Current address: Division of Engineering and Construction Management, John Brown University, 110 Balzer Technology Center, Siloam Springs, AR 72761. Electronic mail: jxu@jbu.edu

histotripsy provides unique advantages compared to other surgical techniques, such as easier monitoring (Kim *et al.*, 2009; Maxwell *et al.*, 2009b; Wang *et al.*, 2009b), precision (Hall *et al.*, 2007), sharp borders (Xu *et al.*, 2004; Parsons *et al.*, 2007), and minimal damage to the intervening region (Parsons *et al.*, 2007; Maxwell *et al.*, 2009a; Maxwell *et al.*, 2009b).

Histotripsy has been tested in lesioning various bulk tissues, such as ventricular myocardium (Parsons *et al.*, 2006; Parsons *et al.*, 2007), muscle (Cooper *et al.*, 2004; Rabkin *et al.*, 2005), liver (Hall *et al.*, 2007; Kim *et al.*, 2009; Xu *et al.*, 2009), kidney (Kim *et al.*, 2009; Wang *et al.*, 2009b; Xu *et al.*, 2009), and prostate tumors (Huber and Debus, 2001). In the pursuit of improved ablation efficiency of cavitation histotripsy, we have varied acoustic parameters, such as PRFs (Xu *et al.*, 2013), exposure time at each treatment location (Xu and Bigelow, 2011), and preconditioning pulses (Xu *et al.*, 2012), to investigate their individual influences on lesion generation. We previously reported that the effective cavitation activity region varies with tissue type, and that lesion dimension generally decreased with increasing tissue stiffness (Xu and Bigelow, 2011). The decline was sharper for relatively lower stiffness (< 100 kPa). We further hypothesized that for certain types of tissue, the delivered amount of acoustic energy is not large enough for cavitation activities to convert cells in treated tissues to acellular slurry prior to their *in vivo* removal by resident phagocytic cells.

To our knowledge, limited study has been devoted thus far to understanding how the ablative effects of histotripsy depend upon the mechanical properties of tissue. Since it is critical to ascertain in the therapy planning stage the proper histotripsy settings for specific tissues, this experimental study was conducted to fill this crucial knowledge gap by examining histotripsy outcome dependence on three mechanical properties—Young's modulus, fracture toughness, and the bending strength of agar samples.

Selection of the three properties was based on the mechanism of tissue disintegration in cavitation histotripsy. Inertial cavitation, characteristic of the violent expansion and rapid collapse of bubbles, creates a transient strain on the surrounding tissue as the fundamental mechanism involved in fractionation or liquefaction. Since a material's restraint on cavitation generation and maintenance is directly related to lesion formation, Young's modulus (associated with axial restraint), and bending strength (associated with transverse restraint) were chosen as directly relevant parameters in this study. Young's modulus describes the tendency of a material to deform along an axis when opposing forces are applied along that axis; bending strength was also quantified describes a material's ability to resist deformation under load. We hypothesized these two properties would be important factors in modulating cavitation. Fracture toughness describes the ability of a material containing a crack to resist fracture. Since HIFU delivers energy into a small focal zone, mechanical scanning of transducer focus or electronic array phasing of transducer elements (or both) generally need to be used during sonication in order to treat a relatively large target region. Normally, the target region is compartmentalized into elements. The already treated compartment may be viewed as a "defect" by the neighboring untreated compartment, leading to our hypothesis that fracture toughness would be a useful measure of a material's resistance to further lesioning damage.

In this study, we used histotripsy to produce six lesions inside each agar sample. For each target region ($4.5\text{ mm} \times 4.5\text{ mm} \times 6\text{ mm}$ cuboid), a raster scanning pattern was utilized to cover a $7 \times 7 \times 3$ mesh. At each treatment location, HIFU was delivered in the form of 5000, 10 000, or 20 000 tone bursts with a 3-ms burst period. Within 3 h after ultrasonic exposures, the three mechanical properties of each agar sample were determined. By comparing lesion volume and bubble cluster dimension among agar samples with different properties, we anticipated identifying the properties playing predominant influences on histotripsy lesion size, and facilitating accurate therapy planning.

II. MATERIALS AND METHODS

A. Material preparation and ultrasound source calibration

Agar phantoms were used to emulate soft organs mainly because of controllability of both their mechanical and acoustic properties (Browne *et al.*, 2003; Madsen *et al.*, 2006). Samples were made by mixing agar powder (Granulated BP1423, Fisher Scientific, Pittsburg, PA) and polyvinyl agar (PVA) powder (R26433, MP Biomedicals, LLC, Solon, OH) into 300 mL boiled distilled water. The weight of the granulated agar powder was either 4 or 9 g while that of PVA powder was 0, 1.5, or 3 g. To solidify the solution and form cylindrical chunks $\sim$4 cm thick and 8 cm in diameter, the solution was stirred thoroughly until turning transparent, was cooled down to room temperature (20 °C), and then was placed in a vacuum chamber (at 25 in. Hg) for 6, 12, or 18 h to dispel gas bubbles. The six weight ratios of the two powders and the three "vacuum durations" led to 18 manufacturing conditions, to differentiate mechanical properties of our tissue mimic. Two agar samples were made for each manufacturing condition to evaluate the dimensional dependence of histotripsy lesions on the properties.

Our 1.1 MHz single-element spherically focused transducer (H-101, Sonic Concepts, Inc., Bothell, WA) was calibrated with a procedure detailed in our earlier work (Xu and Bigelow, 2011). Calibration results indicated that the high-power amplifier (55 dB gain, 1140LA-CI, Electronics & Innovation Ltd., Rochester, NY), when connected to the H-101 transducer and driven at its highest setting of 382.3-V peak-to-peak excitation, could generate peak compressional and rarefactional pressures at the focus of $\sim$102 and 17 MPa, respectively. The equivalent pressure assumed uniform over the transducer surface was determined to be 811 kPa. Acoustic (pulse-average) power output and spatial-peak-pulse-average intensity (I_{SPPA}) for free field were determined with simulation to be 729 W and 41.1 kW/cm^2, respectively.

B. Cavitation histotripsy to agar

In degassed/deionized water, the ultrasound source was positioned above agar. Refer to our earlier publications

(Xu and Bigelow, 2011; Xu *et al.*, 2012; Xu *et al.*, 2013) for diagram of the experimental set-up. Prior to histotripsy, the focus of ultrasound transducer was aligned to the top surface of the sample, using a pulser/receiver (Panametrics 5900PR, Waltham, MA). The transducer (focus) was then lowered 2 cm into the agar, using a computer-controlled positioning system (BiSlide Assemblies, VELMEX Inc., Bloomfield, NY). Before initiating HIFU exposure, the attenuation and speed of sound of the agar were measured by comparing the voltage signals without and with agar phantom in the acoustic propagation path (Bloch, 1998).

HIFU was delivered into individual cuboid confinements of 4.5 mm wide (lateral to the focal plane) and 6 mm deep (axially or along the beam axis). Calibration results indicated the −3 dB (in terms of intensity) beam width in the focal plane and the depth of focus along the beam axis were 1.4 and 9.5 mm, respectively. The presence of agar would not affect them to a considerable degree, as the speed of sound and the attenuation in agar were measured to be negligibly different from water. Considering the size of the focal zone, a mechanical scan of transducer focus was implemented during sonication to treat the aforementioned cuboid region. Regarding the 3-D raster scanning pattern, the axial scan was in the downward direction of moving towards the agar. The scan step sizes in the lateral and axial directions were 0.75 and 3 mm, respectively, bringing the total of treatment locations for each target region to 147. The exposure parameters were coordinated with a waveform generator (Agilent 33220A, Agilent Technologies, Inc., Santa Clara, CA). The theoretical lesion width is the sum of scan length and −3 dB beam width in the focal plane, as the two ends of any scanned border lateral to the focal plane should extend half −3 dB beam width each. This causes the theoretical lesion shape to be a round-cornered square with a 5.9-mm side length. Similarly, the theoretical lesion depth equals the sum of scan length in the axial direction and depth of focus along the beam axis, namely, 15.5 mm. As a result of this beam width effect, the initially targeted region ($4.5 \times 4.5 \times 6$ mm) was effectively elongated slightly in all three directions, yielding a treated cuboid of ∼0.54 mL.

At each treatment location, there was sonication duration of 15, 30, or 60 s. Therefore, the exposure at each treatment location comprised 5000, 10 000, or 20 000 tone bursts, and the exposure time for a single lesion totaled 37, 74, or 147 min. In addition, the exposure consisted of 20-cycle tone bursts with a 333-Hz PRF. Thus, the duty factor was 0.61%, and the spatial-peak-temporal-average intensity (I_{SPTA}) for free field was 249 W/cm^2. Each sample accommodated 6 lesions (with individual target regions spaced 20 mm apart) so 4 repetitions were performed for each of the 54 acoustical/manufacturing conditions.

C. Measurement of lesion dimensions

Upon completion of the six exposures, the agar was cut in half (lateral to the focal plane) and was gently irrigated to remove the exposure-induced slurry. Lesions would appear in the form of holes with clearly demarcated boundaries. The holes were lightly dried with paper towels, and irrigation was repeated as necessary to ensure no slurry left. Since the cut bisected the lesions, the holes could be filled from both sides with food coloring from a 1-mL syringe to approximate each lesion volume. Lesion widths were measured with a digital caliper (Marathon CO030150, Marathon Watch Company Ltd., Richmond Hill, Ontario, Canada). Measurements showed an average discrepancy of 5.3% between the two lesion widths. Since manual slicing could easily engender a slightly oblique cut in the middle of agar, we deemed the overall deviation acceptable and combined the two widths for each lesion for subsequent analysis.

D. Measurement of mechanical properties of agar

Agar properties were measured within 3 h following lesion dimension measurement. During this waiting period, the agar was stored in a refrigerator and doubly bagged to reduce evaporation. In measuring the properties, specimens were taken from the lesion areas (inside the agar). Measuring the properties before sonication would have involved creating lesions close to the edges of the agar if samples were to be taken from the close-to-lesion areas, because it is unlikely to take samples from inside in advance while not damaging the agar. Future studies might wish to quantify the properties before and after sonication, and also immediately above and below (versus on the sides of) the lesion because it is possible that the ultrasound outside the focal zone might also be slightly changing the mechanical properties.

Agar stiffness was measured using standard Hertz contact analysis through a linear translation platform (Thorlabs Inc., Newton, NJ). Its principle is modeling the contact between an elastic sphere (i.e., a load sensor with known properties such as Young's modulus and Poisson's ratio) and an elastic half-space (i.e., agar sample), and then determining Young's modulus of agar by fitting the load-indentation curve. More specifically, agar was moved upward at a constant speed of 0.1 mm/s toward the sensor, with one movement corresponding to one division and 0.001 in. Therefore, the indentation was the displacement difference of the platform and measurement region (on agar surface) after contact. The force was determined through a calibrated linear relationship with voltage signal which was proportional to the displacement of measurement region (as the agar was lifted on the platform). Therefore, a set of platform movement data and voltage data were collected for each of the three measurement region.

Young's moduli of most nonmineralized tissues range from roughly 0.01 to 1000 kPa (Wong *et al.*, 2004; Reilly and Engler, 2009). However, when applying ultrasound histotripsy clinically, one of the most exciting potential applications involves the use of histotripsy in treating liver tumors (Kim *et al.*, 2013; Vlaisavljevich *et al.*, 2013). Therefore, we developed our agar samples to have elastic moduli similar to liver tissue/tumors with value between 27 and 250 kPa. As a comparison, heptocellular carcinoma tumors were reported to have a range of 20.4–75 kPa, and metastatic liver tumors may have a range of 23.6–75 kPa (Masuzaki *et al.*, 2007). Likewise, normal liver tissue ranges from ∼15 kPa to ∼1 MPa depending on the applied strain (Rosen *et al.*, 2008; Umale *et al.*, 2013) while the elasticity of the hepatic veins

and arteries is ~30 kPa at normal blood pressure (Wang *et al.*, 2009a; Li *et al.*, 2012). We did not extend the modulus beyond 250 kPa as our earlier study showed that the therapy became independent of stiffness at higher stiffness values (Xu and Bigelow, 2011).

To quantify fracture toughness, we used a similar setup to measure the critical stress intensity factor at which a thin crack in a single edge notch bending specimen begins to grow (Bower, 2009). The following procedure was used to determine plane strain fracture toughness, K_{Ic}. First, a specimen of 1 cm (thickness B) × 1 cm (width W) × 3 cm was made and fixed to a plastic channel, with 14 mm secured and 16 mm hanging over the edge. Second, a 2-mm (crack length a) incision was made on the dorsal region of the specimen, using a precision knife blade. Third, the specimen was moved toward the sensor at 0.1 mm/s (with a tendency to grow the crack). The platform movement and voltage data were collected every 0.001 in. until a complete fracture occurred. Last, the equation (Bower, 2009) below was used:

$$K_{Ic} = \frac{8F_c}{B}\sqrt{\frac{\pi}{W}}\left[1.6\left(\frac{a}{W}\right)^{1/2} - 2.6\left(\frac{a}{W}\right)^{3/2} + 12.3\left(\frac{a}{W}\right)^{5/2} - 21.2\left(\frac{a}{W}\right)^{7/2} + 21.8\left(\frac{a}{W}\right)^{9/2}\right] = 9.1143F_c\,\text{kPa}\,\text{m}^{1/2}, \quad (1)$$

where F_c in N is the critical load when the crack begins to grow, namely, the peak of the load-displacement curve. As before, force was determined through a calibrated function of voltage. Three specimens were tested for fracture toughness assessment for each agar sample.

Our 36 agar samples were measured to have a range of 0.32–3.18 kPa $m^{1/2}$ (0.585–57.8 J/m^2, see below) for the fracture toughness. The reported toughness values of mammalian tissue make up a wide range, such as 75.8–185.6 J/m^2 for porcine liver (Azar and Hayward, 2008), 164 ± 6 J/m^2 for bovine liver (Gokgol *et al.*, 2012), and 17 000 J/m^2 for dermal porcine tissues (Comley and Fleck, 2010). Note that a fracture mechanics approach based on energy balance was used in the literature, and the corresponding measure of fracture toughness was the work of fracture (denoted γ_{WOF}). On the assumption of plane stress condition, the relationship $\gamma_{WOF} = K_{Ic}^2/2E$ (Broek, 1982; Santos and Rodrigues, 2003) is valid, where E is Young's modulus. This relationship results in the range of 0.585–57.8 J/m^2 for the fracture toughness for our agar. Even though the plane stress condition might be not always met, the above conversion indicates that our agar did not fully represent organs/tissues from the perspective of fracture toughness and that higher values of fracture toughness need to be tested in the future. In later data analysis, the fracture toughness values determined with our technique (rather than the stiffness-based energy technique) were used throughout, with the aim of separating the effects of Young's modulus and fracture toughness with regard to histotripsy outcome.

To measure bending strength, specimens of 1 cm (thickness B) × 1 cm (width W) × 4 cm (length L) were used in a standard three-point bending setup, where the two ends were secured (using two plastic channels) and a vertical load of the fixed sensor was applied at the middle of the moving specimen. The bending strength, formulated as $\sigma = 3FL/2WB^2 = 60F$ kPa, where F in N is the load at the fracture point, was determined to range from 0.58 to 2.93 kPa. For homogeneous and isotropic materials, bending strength is identical to tensile strength. In regard to the tensile strength, aorta was reported to have a range of 300–800 kPa (Silver *et al.*, 1989), and human skin was determined to have a mean of 21.6 ± 8.4 MPa (Annaidh *et al.*, 2012). Thus the bending strength of our agar was significantly lower and additional tests should be conducted in the future at higher values.

III. RESULTS

A. Acoustical properties of agar samples

At 1.1 MHz, both the speed of sound traveling through our agars and the associated attenuation were measured to be negligibly different from water. This implied that our agar was a nearly lossless phantom with controllable mechanical properties. Since we wanted to focus on the mechanical effects of cavitation-based histotripsy, using lossy agar would have complicated our assessment of the mechanical damage in agar, as thermal lesions in lossy agar would have disparate features from thermal lesions in tissue. In short, lossless agar is the best medium identified to date for testing cavitation-based histotripsy, especially when only the quantification of mechanical damage is intended.

B. Mechanical properties of agar samples

Figure 1 shows the load-indentation curves used to determine Young's modulus (E), bending strength (σ), and fracture toughness (K) for a sample that was made of 9 g of agar and 3 g of PVA with the solution placed in the vacuum chamber for 12 h. Corresponding to the nine curves, the three values for Young's modulus are 181.8, 183.1, and 175.1 kPa; the bending strength values are 1.93, 1.88, and 1.84 kPa (note that the right y axis and the middle three curves with

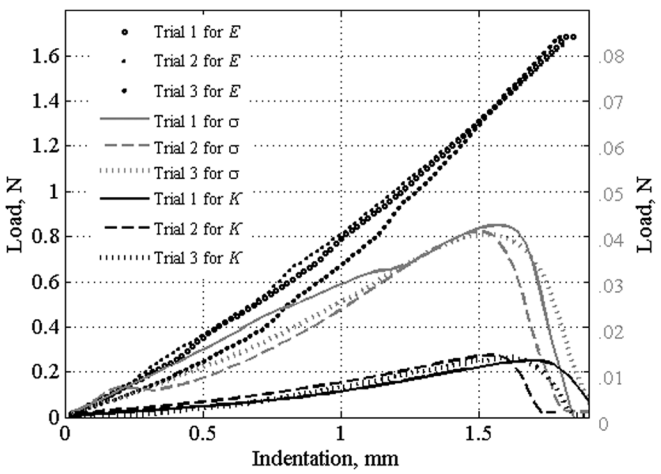

FIG. 1. Property determination through load-indentation curves, for a sample made of 9 g of agar and 3 g of PVA.

TABLE I. Young's modulus (in kPa) of agar samples.

Agar/PVA	4 g/ 0 g	4 g/ 1.5 g	4 g/ 3 g	9 g/ 0 g	9 g/ 1.5 g	9 g/ 3 g
6 h	27.2, 34.6	38.5, 42.3	41.1, 49.7	87.6, 92.5	101.6, 99.3	116.5, 106.8
12 h	49.1, 55.7	58.4, 61.2	69.3, 70.7	154.5, 156.1	164.1, 149.8	176.7, 180.0
18 h	72.1, 77.9	82.6, 80.8	83.1, 87.5	215.6, 224.2	229.6, 236.9	235.3, 250.4

lighter color are used for this property); the fracture toughness values are 2.28, 2.50, and 2.40 kPa $m^{1/2}$. The mechanical properties of all agar samples are shown in Tables I–III, where columns represent the variation of agar and PVA weights and rows list the vacuum duration. Comparison between 4 and 9 g counterparts indicates that the added agar powder led to an evident increase in Young's modulus but a decrease in the other two properties, whereas the increment of PVA powder weight (with the same amount of agar powder) resulted in a gain in all three properties. Meanwhile, the elongated vacuum duration tended to increase all properties.

C. The effects of mechanical properties on lesion volume

All the sonications created lesions with clear boundaries inside the agar samples. Using the methods described earlier, we estimated the volume and two widths (perpendicular to ultrasound beam) for each lesion. In identifying the possible relationships between lesion dimensions and mechanical properties, statistical properties related to linear correlation were used. Specifically, for each of the three exposure conditions, the correlation coefficient and the corresponding p-value (for testing the hypothesis of no correlation) were determined with MATLAB for each of the three mechanical-property arrays, compared to the lesion volume, equivalent bubble cluster widths or equivalent lengths.

Generally, pairs of datasets are associated with correlation coefficients, but these coefficients by themselves may neglect the effect of outliers. (Scatterplots of Anscombe's quartet is an example.) Hence we first performed visual examination of our data graphs, followed by correlation analysis. Figure 2 presents the change of lesion volume (V) with Young's modulus (E), also showing bending strength (σ) in panel (a), and fracture toughness (K) in panel (b). Both fracture toughness and bending strength graphically appeared to exhibit a nominal influence on the volume, as the profiles along different values of either property seems the same. This statistically verified observation with 15-s exposures applied to all three exposure times.

Interpretation of the correlation coefficients in Fig. 2 were that 69% (coefficient of determination $= R^2$ value $= 0.83^2$) of the variations in the lesion volume can be accounted for by differences in the Young's modulus while only 2% ($= 0.13^2$) by those in the bending strength and 2% ($= 0.14^2$) by those in the fracture toughness. In practice, there was a significant correlation between Young's modulus and lesion volume, with the lowest correlation coefficient ($r = 0.72$, $p < 0.001$) occurring at 60-s-exposure datasets. In contrast, among the relationships of lesion volume with the other properties, the highest correlation coefficient was merely 0.19 ($p = 0.26$), and occurred with bending strength and at 60-s-exposure datasets. As confirmed by the correlation analysis, the plots of lesion volume against bending strength and fracture toughness were irregular and did not show a strong trend in any particular direction. Therefore, we computed a single-variable power fit (excluding σ and K) for the decreasing relationship with E for each of the three exposure times, as summarized in Table IV.

D. The effects of mechanical properties on equivalent bubble cluster width

Activity of bubble clusters is believed to cause damage to tissue. Quantification of lesion widths enabled one to observe the effects of the mechanical properties on the equivalent width and length of the bubble cluster. The measurement principles for them are as follows. First, corresponding to each exposure condition, the equivalent width should be consistent and identical in all radial directions. The two ends of any scanned border lateral to the focal plane should thus extend half the width of the bubble cluster. Subtracting the lateral scan length (i.e., 4.5 mm) from the lesion width measurements leads to the equivalent bubble cluster width for each treatment location. Likewise, the equivalent bubble cluster length was assumed to be consistent for any given exposure condition. Hence the equivalent length could be estimated by dividing the volume by the two widths of a lesion (i.e., approximating the lesion cross-sectional area as rectangular) and then subtracting this quotient by the axial scan length (i.e., 6 mm).

As before, the data were visually examined, followed by calculation of correlations, in exploring the effects of the mechanical properties on the two equivalent bubble cluster dimensions. For all three exposure times, the change of equivalent bubble cluster width (w) followed a tendency

TABLE II. Bending strength (in kPa) of agar samples.

Agar/PVA	4 g/0 g	4 g/1.5 g	4 g/3 g	9 g/0 g	9 g/1.5 g	9 g/3 g
6 h	0.72, 0.80	1.52, 1.38	1.93, 2.01	0.58, 0.66	1.11, 1.18	1.54, 1.52
12 h	1.02, 1.13	1.68, 1.54	2.51, 2.40	0.69, 0.88	1.32, 1.43	1.96, 1.88
18 h	1.32, 1.46	2.26, 2.10	2.93, 2.79	1.02, 1.15	1.60, 1.71	2.21, 2.26

TABLE III. Fracture toughness (in kPa $m^{1/2}$) of agar samples.

Agar/PVA	4 g/0 g	4 g/1.5 g	4 g/3 g	9 g/0 g	9 g/1.5 g	9 g/3 g
6 h	0.89, 0.96	1.33, 1.42	1.94, 2.06	0.32, 0.41	0.84, 0.97	1.31, 1.52
12 h	1.03, 1.15	1.80, 1.88	2.61, 2.73	0.96, 0.93	1.59, 1.64	2.23, 2.38
18 h	1.18, 1.23	2.39, 2.54	2.98, 3.18	0.91, 1.02	1.75, 1.87	2.46, 2.67

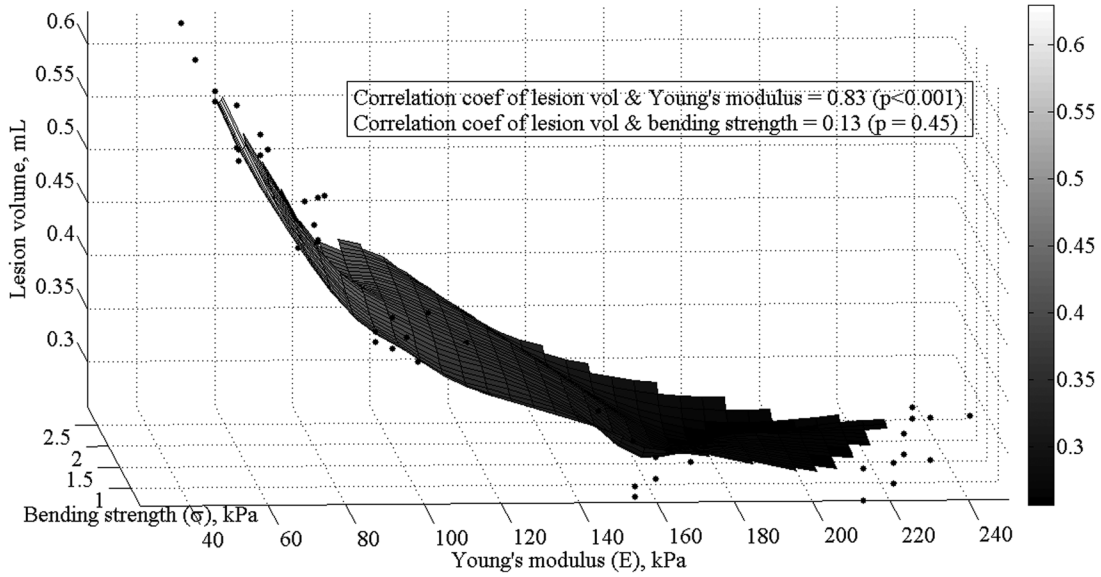

(a)

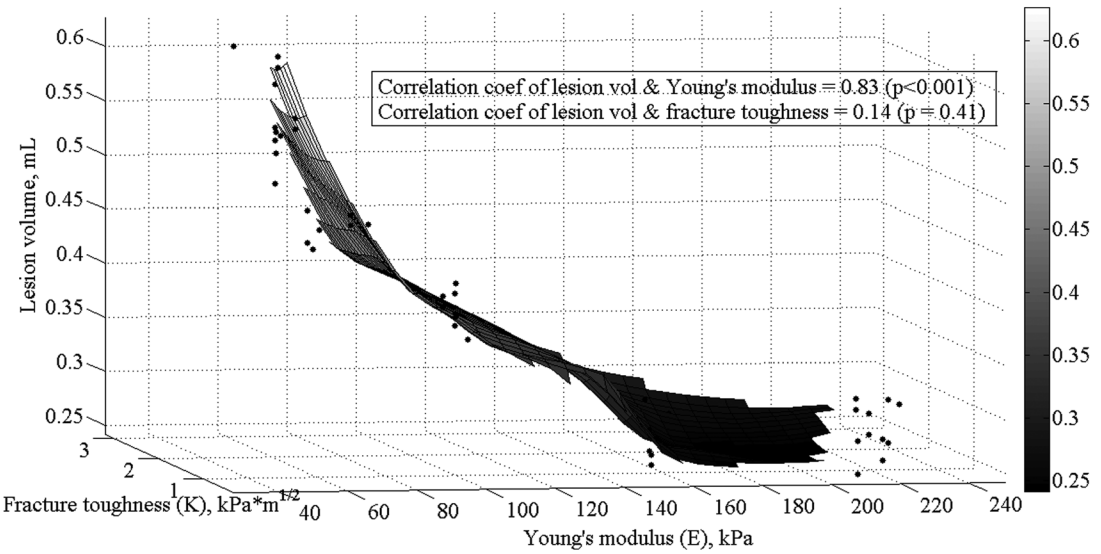

(b)

FIG. 2. Surface plot (after 2-D fitting) of lesion volumes, corresponding to 15-s exposure at each treatment location.

similar to that for the lesion volume, as there was a significant inverse correlation ($r > 0.66$, $p < 0.001$) between w and Young's modulus (E) (Table IV). In contrast, the correlations of w with the other two mechanical properties had correlation coefficients lower than 0.12 ($p > 0.49$). Using the 30-s exposure time as an example: 44% ($=0.66^2$) of the w variations can be accounted for by differences in E, whereas only 0.3% ($=0.05^2$) by those in bending strength (σ) and 0.09% ($=0.03^2$) by those in fracture toughness (K). Graphically, the profiles along different values of σ or K did not show a significant trend.

Since all w values were larger than 2.67 mm (with the minimum occurring with the 15-s exposure time), bubble clusters laterally extended beyond −3 dB beam width (i.e., 1.4 mm). A more profound meaning is that the bubble cluster was always wider than the lateral scan step size of 0.75 mm, as might be expected. It can be inferred that with our acoustic setting, there was always a superimposition from the

TABLE IV. Correlation of lesion volume and equivalent bubble cluster dimensions with Young's modulus.

Time	Lesion volume Power fit (SSE; R^2)	Bubble cluster width Power fit (SSE; R^2)	Bubble cluster length Power fit (SSE; R^2)
15 s	$V = 8.63\,E^{-0.668}$(0.059; 0.975)	$w = 18.9\,E^{-0.438}$ (10.3; 0.770)	$l = 141\,E^{-0.922}$ (75.5; 0.681)
30 s	$V = 3.82\,E^{-0.466}$(0.271; 0.835)	$w = 21.5\,E^{-0.432}$ (10.7; 0.807)	$l = 14.8\,E^{-0.442}$ (95.3; 0.252)
60 s	$V = 8.47\,E^{-0.601}$(0.368; 0.890)	$w = 23.4\,E^{-0.419}$ (10.3; 0.846)	$l = 25.2\,E^{-0.497}$ (40.4; 0.533)

HIFU-induced bubble clusters at any two adjacent treatment locations. This possesses clinical significance, as a bubble cluster narrower than the scan step size would possibly leave untreated regions in the targeted volume.

E. The effects of mechanical properties on equivalent bubble cluster length

There was a significant correlation ($r > 0.65$, $p < 0.001$) between equivalent bubble cluster length l (along the beam axis and perpendicular to the focal plane) and E. The correlations of l with the other two properties were not significant ($r < 0.24$, $p > 0.15$). For example, for the 15-s exposure time, 72% ($=0.85^2$) of the l variations could be accounted for by differences in E while only 3% ($=0.17^2$) by those in σ and 6% ($=0.24^2$) in K. Correlations of l with E in the form of power fit are contained in Table IV. It is worth noting that our exposure conditions never produced bubble clusters longer than 9.5 mm (i.e., the theoretical axial confinement). Nonetheless, within sufficiently soft tissue, the bubble cluster activity region would theoretically possibly exceed the −3 dB axial depth of focus along the beam.

F. The effects of exposure time on lesion volume

Since lesion dimension was significantly correlated only with Young's modulus, we focused further analysis on the agar samples with close Young's moduli in order to illuminate the impact of acoustic conditions on the efficiency of lesion formation. This is important because the ultimate goal of histotripsy is to develop a safe, efficient, and precise surgical tool. Among various possible study variables associated with exposure conditions, we selected the exposure time at each treatment location and varied this time between 15, 30, and 60 s to explore the previously observed primary dependence of histotripsy ablation on Young's modulus. For this analysis, a group of six agar samples with 77.9–87.6 kPa stiffness (11% maximum change) and another group of five samples with 215.6–236.9 kPa stiffness (9% change) were selected to explore the effect of exposure time on lesion volume, equivalent bubble cluster width and length. A one-tailed student's t test was run for statistical analysis. In addition, the Bonferroni correction was applied to avoid type I error (characteristic of artificial significance for difference), lowering the critical value of significance level (at an alpha value of 0.05) by a factor of 3 to 0.017.

Figure 3 displays an ascending trend of lesion volume with the exposure time at each treatment location. Since the highest of the p-values for both agar groups was $p < 0.0006$, the lesion volume increased significantly with the exposure time. Also, the volumes in Fig. 3 are commonly small because the selected samples had a relatively large stiffness, whereas it is worth noting that the lesion volume could exceed the theoretical confinement of 0.54 mL (corresponding to the target region).

G. The effects of exposure time on equivalent bubble cluster width

Figure 4 displays a significantly ascending trend ($p < 0.0017$, $n = 12$ or 10) of the equivalent width (w) with

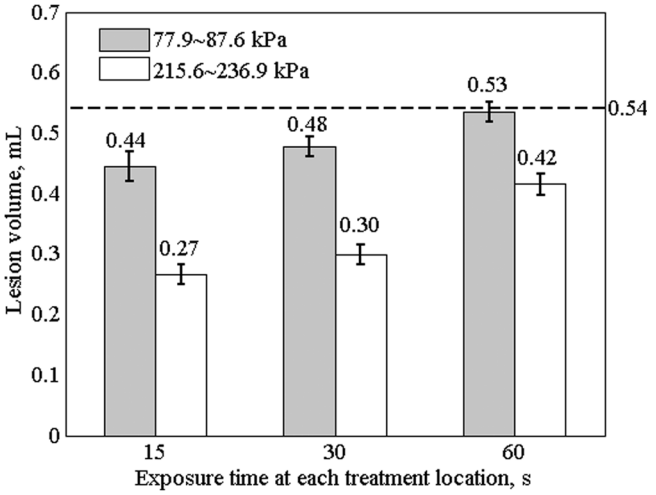

FIG. 3. Variation of lesion volume with exposure time, for agar groups with average Young's moduli of 83.3 and 228.3 kPa.

the exposure time at each treatment location. While a similar tendency was observed earlier with lesion volume (in Fig. 3), the bubble clusters exceeded the theoretical lateral confinement of 1.4 mm at all times (different from the volume performance). In contrast to the lesion volume data (Fig. 3), equivalent widths for the two groups are comparatively close. This implies that the alteration of histotripsy ablation might primarily hinge on the axial extension of bubble clusters. This is in agreement with the previous observation that Young's modulus has a dominating effect in histotripsy's ablative ability, since this modulus was also closely associated with the material's performance in the axial direction. Thus this observation may reflect a restraining effect against bubble cluster activity, correlated with Young's modulus.

H. The effects of exposure time on equivalent bubble cluster length

Figure 5 further investigates this idea by showing a sharper contrast of equivalent bubble cluster lengths (l) between two selected agar groups, and highlighting the remarkable influence of stiffness on histotripsy's ablative

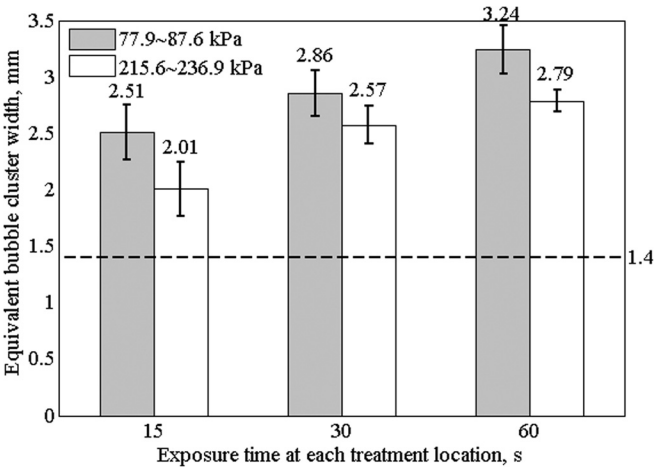

FIG. 4. Variation of equivalent bubble cluster width with exposure time, for agar groups with average Young's moduli of 83.3 and 228.3 kPa.

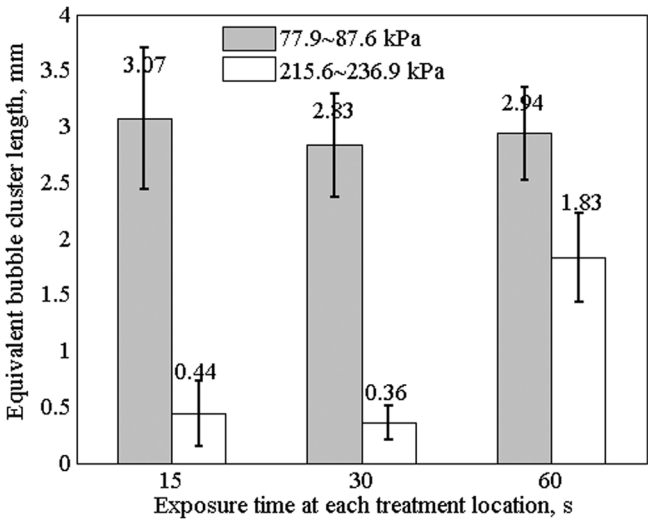

FIG. 5. Variation of equivalent bubble cluster length with exposure time, for agar groups with average Young's moduli of 83.3 and 228.3 kPa.

ability. The three exposure times were not significantly different ($p > 0.15$, $n = 12$ or 10) in terms of producing l, with the exception of the 60-s exposures in the second group ($p < 0.0001$, $n = 10$). These results show that the increase in bubble cluster length is modulated differently than the bubble cluster width, as exposure time changes. Future studies should look at whether a shorter exposure time would lead to a close equivalent bubble cluster length, and whether there is a relationship between exposure time and the cluster length (for a certain stiffness).

IV. DISCUSSION/CONCLUSIONS

A total of 216 HIFU exposures were administered to targeted regions of 0.54 mL inside agar gels. For each exposure, discrete treatment locations formed a 3D mesh while 20-cycle HIFU pulses were delivered at each treatment location. These pulses excited and maintained bubble cavitation activities, resulting in tissue fractionation. Hence the bubble cluster region is directly related to the ablative ability of the cavitation histotripsy. Our work indicated that even though lesions were successfully created under the same acoustic conditions through histotripsy liquefaction, the lesion volumes varied depending on the mechanical properties of the tissue-mimicking agar phantom. Furthermore, the equivalent dimension of the active bubble cluster that was responsible for the liquefaction was quantified for each exposure (and each agar sample). Our most important finding is that Young's modulus appears to be much more important than bending strength or fracture toughness in predicting the lesion volume. In our experiment, only Young's modulus appeared to be significantly correlated with lesion volume and equivalent bubble cluster width w (perpendicular to the focal plane) and length l (along the beam axis).

Therapy precision is one of the most important factors for histotripsy. Improved precision is desired in therapy because of the potential for reducing the risk of damaging tissue in the vicinity of sensitive structures. Since all bubble clusters under our acoustic settings were wider than the lateral step size of 0.75 mm, there were no untreated regions in the targeted volume. In this regard, it is worthwhile to point out that the significant gain in the equivalent bubble cluster width due to the elongated exposure time may be not always desirable from a clinical perspective. In other words, shorter exposures at each treatment location (yielding narrower bubble clusters) might assist with precision control over lesion dimension on the focal plane, not to mention the benefit of decreased therapy time.

In addition, precision improvement is viable only if the cavitation-based histotripsy procedure can be monitored in real time. Since Young's modulus was found to determine the ablative ability of histotripsy, any acoustic imaging method based on stiffness measurement (e.g., elastography) would be perfect to use in combination with histotripsy. This combination, for instance, can be easily implemented by using a therapy transducer and an imaging probe together to minimize the medical expenditure. This is another advantage of histotripsy over the traditional thermal-ablation-based HIFU procedure.

Limitations and prospects of our study should be noted. First, given the high frequency of cavitation activities, dynamic fracture toughness testing would give better fidelity to the histotripsy damage measurements involving fatigue defects. Few studies have examined fracture toughness testing with respect to the sensitivity of the agar to loading conditions such as loading speed. Furthermore, we did not examine the correlation between static and dynamic fracture toughness values in this study. Therefore, it would be useful for future studies to incorporate this additional parameter for additional comparisons.

Second, since our agar represented a limited range of tissues from the perspective of bending strength and fracture toughness, the conclusions drawn from this study may not be generalized to all soft tissues. It is possible that these two properties do affect the lesion formation in very soft or very hard tissues, outside the range of our experiment. In the future, the physical cross-linking approach for agar production might be able to yield higher bending strength and fracture toughness in order to extend to the range for those soft tissues.

Similarly, the use of extreme exposure conditions might render our findings invalid. For example, excessively short exposures possibly would not lesion agar at all; excessively long exposures would create similar size of lesions inside all the agar samples used. The former would make the concept of equivalent bubble cluster dimension inapplicable, and the latter would deceitfully lead to the conclusion that the ablative ability of cavitation-based histotripsy is independent of tissue properties. Nonetheless, either case would produce meaningless clinical effects, namely, no lesions or unacceptably long exposures. Thus this study did not attempt to encompass those extreme conditions.

Last, only the quantification of mechanical damage was intended in this cavitation-based histotripsy study. It is necessary for future study to test thermal damage and investigate the effects of acoustic properties on lesion dimension by using tissue with varying attenuations while accurately quantifying the Young's modulus.

In summary, our finding in this study that Young's modulus is crucial for predicting the ablative ability of histotripsy is an important step toward increasing the precision of this surgical technique. Our secondary finding that exposure time differentially modulates the axial depth compared to the cross-sectional area of histotripsy lesions will aid therapists in their surgical planning. The corollary implication of these results, that elastography or other stiffness-based real-time imaging modality pairs ideally with histotripsy, will help to provide the basis for the next-generation extremely safe and accurate noninvasive surgical tools of the future.

ACKNOWLEDGMENT

The authors thank Dr. Joshua Soneson at the Division of Solid and Fluid Mechanics at FDA for providing code which solves the axisymmetric KZK equation for HIFU beams and was modified for our source calibration.

Annaidh, A. N., Bruyere, K., Destrade, M., Gilchrist, M. D., and Ottenio, M. (**2012**). "Characterising the anisotropic mechanical properties of excised human skin," J. Mech. Behav. Biomed. Mater. **5**, 139–148.

Azar, T., and Hayward, V. (**2008**). "Estimation of the fracture toughness of soft tissue from needle insertion," in *Biomedical Simulation, Proceedings of the Fourth International Symposium*, edited by F. Bello and P. J. Edwards (Springer, Berlin, 2008), Vol. 5104, pp. 166–175.

Bigelow, T. A., Northagen, T., Hill, T. M., and Sailer, F. C. (**2009**). "The destruction of *Escherichia coli* biofilms using high-intensity focused ultrasound," Ultrasound Med. Biol. **35**, 1026–1031.

Blana, A., Walter, B., Rogenhofer, S., and Wieland, W. F. (**2004**). "High-intensity focused ultrasound for the treatment of localized prostate cancer: 5-year experience," Urology **63**, 297–300.

Bloch, S. (**1998**). *Ultrasonic Tissue Characterization: Towards High-intensity Focused Ultrasound Treatment Monitoring* (University of Washington Press, Seattle).

Bower, A. F. (**2009**). *Applied Mechanics of Solids* (Chemical Rubber Company [CRC] Press, Boca Raton, FL), Chap. 9.

Broek, D. (**1982**). *Elementary Engineering Fracture Mechanics* (Springer, New York), p. 469.

Browne, J. E., Ramnarine, K. V., Watson, A. J., and Hoskins, P. R. (**2003**). "Assessment of the acoustic properties of common tissue-mimicking test phantoms," Ultrasound Med. Biol. **29**, 1053–1060.

Canney, M. S., Khokhlova, V. A., Bessonova, O. V., Bailey, M. R., and Crum, L. A. (**2010**). "Shock-Induced Heating and Millisecond Boiling in Gels and Tissue Due to High Intensity Focused Ultrasound," Ultrasound Med. Biol. **36**, 250–267.

Clarke, R. L., and Haar, G. R. T. (**1997**). "Temperature rise recorded during lesion formation by high-intensity focused ultrasound," Ultrasound Med. Biol. **23**, 299–306.

Comley, K., and Fleck, N. A. (**2010**). "The toughness of adipose tissue: Measurements and physical basis," J. Biomech. **43**, 1823–1826.

Cooper, M., Xu, Z., Rothman, E. D., Levin, A. M., Advincula, A. P., Fowlkes, J. B., and Cain, C. A. (**2004**). "Controlled ultrasound tissue erosion: the effects of tissue type, exposure parameters and the role of dynamic microbubble activity," in *IEEE International Ultrasonics, Ferroelectrics, and Frequency Control Joint 50th Anniversary Conference*, pp. 1808–1811.

Damianou, C., Pavlou, M., Velev, O., Kyriakou, K., and Trimikliniotis, M. (**2004**). "High intensity focused ultrasound ablation of kidney guided by MRI," Ultrasound Med. Biol. **30**, 397–404.

Gateau, J., Aubry, J.-F., Chauvet, D., Boch, A.-L., Fink, M., and Tanter, M. (**2011**). "In vivo bubble nucleation probability in sheep brain tissue," Phys. Med. Biol. **56**, 7001–7015.

Gokgol, C., Basdogan, C., and Canadinc, D. (**2012**). "Estimation of fracture toughness of liver tissue: Experiments and validation," Med. Eng. Phys. **34**, 882–891.

Hall, T. L., Fowlkes, J. B., and Cain, C. A. (**2007**). "A real-time measure of cavitation induced tissue disruption by ultrasound imaging backscatter reduction," IEEE Trans. Ultrason. Ferroelectr. Freq. Control **54**, 569–575.

Huber, P. E., and Debus, J. (**2001**). "Tumor cytotoxicity in vivo and radical formation in vitro depend on the shock wave-induced cavitation dose," Rad. Res. **156**, 301–309.

Kim, Y., Fifer, C. G., and Gelehrter, S. K. (**2009**). "Non-invasive fetal therapy using histotripsy: feasibility study in the sheep model," *IEEE International Ultrasonics Symposium Proceedings*, pp. 228–231.

Kim, Y., Fifer, C. G., Gelehrter, S. K., Owens, G. E., Berman, D. R., Vlaisavljevich, E., Allen, S. P., Ladino-Torres, M. F., and Xu, Z. (**2013**). "Developmental impact and lesion maturation of histotripsy-mediated non-invasive tissue ablation in a fetal sheep model," Ultrasound Med. Biol. **39**, 1047–1055.

Li, J., Li, W., Song, J., Zhang, H., Yu, M., He, X., Wang, M., Wang, H., and Huang, T. (**2012**). "Effect of sex on biomechanical properties of the proper hepatic artery in pigs and humans for liver xenotransplant," Exp. Clin. Transplant **10**, 356–362.

Madsen, E. L., Hobson, M. A., Shi, H., Varghese, T., and Frank, G. R. (**2006**). "Stability of heterogeneous elastography phantoms made from oil dispersions in aqueous gels," Ultrasound Med. Biol. **32**, 261–270.

Masuzaki, R., Tateishi, R., Yoshida, H., Sato, T., Ohki, T., Goto, T., Yoshida, H., Sato, S., Sugioka, Y., Ikeda, H., Shiina, S., Kawabe, T., and Omata, M. (**2007**). "Assessing liver tumor stiffness by transient elastography," Hepatol. Int. **1**, 394–397.

Maxwell, A., Sapozhnikov, O., Bailey, M., Crum, L., Xu, Z., Fowlkes, B., Cain, C., and Khokhlova, V. (**2012**). "Disintegration of tissue using high intensity focused ultrasound: Two approaches that utilize shock waves," Acoust. Today **8**, 24–37.

Maxwell, A. D., Cain, C. A., and Duryea, A. P. (**2009a**). "Noninvasive thrombolysis using pulsed ultrasound cavitation therapy—Histotripsy," Ultrasound Med. Biol. **35**, 1982–1994.

Maxwell, A. D., Owens, G., and Gurm, H. S. (**2009b**). "In-vivo study of non-invasive thrombolysis by histotripsy in a porcine model," in *IEEE International Ultrasonics Symposium Proceedings*, pp. 220–223.

Orvieto, M. A., Zorn, K. C., Lyon, M. B., Tolhurst, S. R., Rapp, D. E., Seip, R., Sanghvi, N., and Shalhav, A. (**2009**). "High intensity focused ultrasound renal tissue ablation; a laparoscopic porcine model," J. Urology **181**, 861–866.

Parsons, J. E., Cain, C. A., Abrams, G. D., and Fowlkes, J. B. (**2006**). "Pulsed cavitational ultrasound therapy for controlled tissue homogenization," Ultrasound Med. Biol. **32**, 115–129.

Parsons, J. E., Cain, C. A., and Fowlkes, J. B. (**2007**). "Spatial variability in acoustic backscatter as an indicator of tissue homogenate production in pulsed cavitational ultrasound therapy," IEEE Trans. Ultrason. Ferroelectr. Freq. Control **54**, 576–590.

Rabkin, B. A., Zderic, V., and Vaezy, S. (**2005**). "Hyperecho in ultrasound images of HIFU therapy: Involvement of cavitation," Ultrasound Med. Biol. **31**, 947–956.

Reilly, G. C., and Engler, A. J. (**2010**). "Intrinsic extracellular matrix properties regulate stem cell differentiation," J. Biomech. **43**, 55–62.

Rosen, J., Brown, J. D., De, S., Sinanan, M., and Hannaford, B. (**2008**). "Biomechanical properties of abdominal organs in vivo and postmortem under compression loads," J. Biomech. Eng. **130**, 021020–021020.

Santos, S. F. D., and Rodrigues, J. D. A. (**2003**). "Correlation between fracture toughness, work of fracture and fractal dimensions of alumina-mullite-zirconia composites," Mater. Res. **6**, 219–226.

Silver, F. H., Christiansen, D. L., and Buntin, C. M. (**1989**). "Mechanical properties of the aorta: A review," Crit. Rev. Biomed. Eng. **17**, 323–358.

Uchida, T., Muramoto, M., Kyunou, H., Iwamura, M., Egawa, S., and Koshiba, K. (**1998**). "Clinical outcome of high-intensity focused ultrasound for treating benign prostatic hyperplasia: Preliminary report," Urology **52**, 66–71.

Umale, S., Deck, C., Bourdet, N., Dhumane, P., Soler, L., Marescaux, J., and Willinger, R. (**2013**). "Experimental mechanical characterization of abdominal organs: Liver, kidney & spleen," J. Mech. Behav. Biomed. Mater. **17**, 22–33.

Vlaisavljevich, E., Kim, Y., Allen, S., Owens, G., Pelletier, S., Cain, C., Ives, K., and Xu, Z. (**2013**). "Image-guided non-invasive ultrasound liver ablation using histotripsy: Feasibility study in an in vivo porcine model," Ultrasound Med. Biol. **39**, 1398–1409.

Wang, P. J., Li, W. C., Xi, G. M., Wang, H. Q., Zhang, Z. H., Yao, B. C., Tang, W., Deng, Z. H., and Zhang, X. H. (**2009a**). "Biomechanical study of hepatic portal vein in humans and pigs and its value in liver transplantation," Transplant. Proc. **41**, 1906–1910.

Wang, T. Y., Maxwell, A. D., Park, S., Xu, Z., Fowlkes, J. B., and Cain, C. A. (**2010**). "Why are short pulses more efficient in tissue erosion using

pulsed cavitational ultrasound therapy (histotripsy)?," AIP Conf. Proc. **1215**, 40–43.
Wang, T.-Y., Xu, Z., and Winterroth, F. (**2009b**). "Quantitative ultrasound backscatter for pulsed cavitational ultrasound therapy—Histotripsy," IEEE Trans. Ultrason. Ferroelectr. Freq. Control **56**, 995–1005.
Wong, J. Y., Leach, J. B., and Brown, X. Q. (**2004**). "Balance of chemistry, topography, and mechanics at the cell–biomaterial interface: Issues and challenges for assessing the role of substrate mechanics on cell response," Surf. Sci. Biosurf. V Funct. Polym. Surf. Biotechnol. **570**, 119–133.
Xu, J., and Bigelow, T. A. (**2011**). "Experimental investigation of the effect of stiffness, exposure time and scan direction on the dimension of ultrasound histotripsy lesions," Ultrasound Med. Biol. **37**, 1865–1873.
Xu, J., Bigelow, T. A., and Lee, H. (**2013**). "Effect of pulse repetition frequency and scan step size on the dimensions of the lesions formed in agar by HIFU histotripsy," Ultrasoinics **53**, 889–896.
Xu, J., Bigelow, T. A., and Riesberg, G. M. (**2012**). "Impact of preconditioning pulse on lesion formation during high-intensity focused ultrasound histotripsy," Ultrasound Med. Biol. **38**, 1918–1929.
Xu, Z., Fan, Z., Hall, T. L., Winterroth, F., Fowlkes, J. B., and Cain, C. A. (**2009**). "Size measurement of tissue debris particles generated from pulsed ultrasound cavitational therapy—Histotripsy," Ultrasound Med. Biol. **35**, 245–255.
Xu, Z., Hall, T. L., Fowlkes, J. B., and Cain, C. A. (**2007a**). "Optical and acoustic monitoring of bubble cloud dynamics at a tissue-fluid interface in ultrasound tissue erosion," J. Acoust. Soc. Am. **121**, 2421–2430.
Xu, Z., Ludomirsky, A., and Eun, L. Y. (**2004**). "Controlled ultrasound tissue erosion," IEEE Trans. Ultrason. Ferroelectr. Freq. Control **51**, 726–736.
Xu, Z., Raghavan, M., Hall, T. L., Chang, C.-W., Mycek, M.-A., Fowlkes, J. B., and Cain, C. A. (**2007b**). "High speed imaging of bubble clouds generated in pulsed ultrasound cavitational therapy—Histotripsy," IEEE Trans. Ultrason. Ferroelectr. Freq. Control **54**, 2091–2101.